Iterative blind deconvolution algorithm applied to phase retrieval

J. H. Seldin and J. R. Fienup

Optical Science Laboratory, Advanced Concepts Division, Environmental Research Institute of Michigan, P.O. Box 8618, Ann Arbor, Michigan 48107

Received July 29, 1989; accepted October 24, 1989

The iterative blind deconvolution algorithm proposed by Ayers and Dainty [Opt. Lett. **13**, 547 (1988)] and improved on by Davey *et al.* [Opt. Commun. **69**, 353 (1989)] is applied to the problem of phase retrieval, which is a special case of the blind deconvolution problem. A close relationship between this algorithm and the error-reduction version of the iterative Fourier-transform phase-retrieval algorithm is shown analytically. The performance of the blind deconvolution algorithm is compared with the error-reduction and hybrid input–output versions of the iterative Fourier-transform algorithm by reconstruction experiments on real-valued, nonnegative images with and without noise.

1. INTRODUCTION

Blind deconvolution is the problem of finding two unknown functions, $f(\bar{x})$ and $g(\bar{x})$, from a noisy measurement, $c(\bar{x})$, of the convolution of these functions, defined as

$$c(\bar{x}) = \int_{-\infty}^{\infty} f(\bar{x}')g(\bar{x} - x')\mathrm{d}x' + n(\bar{x})$$

$$= f(\bar{x}) * g(\bar{x}) + n(\bar{x}), \tag{1}$$

or in the Fourier domain as

$$C(\bar{u}) = F(\bar{u})G(\bar{u}) + N(\bar{u}), \tag{2}$$

where C, F, G, and N are the Fourier transforms of c, f, g, and n, respectively. Ayers and Dainty[1] recently proposed a practical, two-dimensional blind deconvolution algorithm for the noise-free case, where the additive noise term $n(\bar{x}) = 0$.

In this paper we apply the Ayers–Dainty (AD) algorithm to the phase-retrieval problem, in which we desire to recover an image, $f(\bar{x})$, from the modulus, $|F(\bar{u})|$, of its Fourier transform:

$$F(\bar{u}) = |F(\bar{u})| \exp[i\psi(\bar{u})] = \mathcal{F}[f(\bar{x})]$$

$$= \int_{-\infty}^{\infty} f(\bar{x})\exp[-i2\pi(\bar{u} \cdot x)]\mathrm{d}x. \tag{3}$$

Phase retrieval is equivalent to the reconstruction of the Fourier phase, $\psi(\bar{u})$, from the Fourier modulus and to the reconstruction of $f(\bar{x})$ or $\psi(\bar{u})$ from the autocorrelation function:

$$r(\bar{x}) = \int_{-\infty}^{\infty} f(\bar{x}')f^*(\bar{x}' - x)\mathrm{d}x'$$

$$= \mathcal{F}^{-1}[F(\bar{u})F^*(\bar{u})] = \mathcal{F}^{-1}[|F(\bar{u})|^2]. \tag{4}$$

The phase-retrieval problem arises in several disciplines including optical and radio astronomy, wave-front sensing, holography, and remote sensing.

Comparing Eqs. (1) [with $n(\bar{x}) = 0$] and (4), we find that phase retrieval can be considered a special case of blind deconvolution, in which we deconvolve $f(\bar{x})$ and $f^*(-\bar{x})$ from $r(\bar{x})$. Because the AD algorithm represents a new, practical algorithm for blind deconvolution, we will apply it to phase retrieval and compare it with two existing phase-retrieval algorithms. We will begin by describing the AD algorithm and adaptations of the algorithm appropriate for phase retrieval. Because its structure closely resembles that of the error-reduction (ER) algorithm commonly used for phase retrieval,[2–4] the AD algorithm is compared both analytically and experimentally with ER. The performance of both of these algorithms is compared with the faster hybrid input–output (HIO) algorithm[2–4] for real, nonnegative objects for the cases of known and unknown support, using Fourier intensity data with different levels of additive Gaussian noise.

2. DESCRIPTION OF THE ALGORITHM

A. Blind Deconvolution

The AD blind deconvolution algorithm[1] (Fig. 1) alternates between the object domain and the Fourier domain, enforcing known constraints in each domain. Object-domain constraints such as support and nonnegativity are combined with the Fourier-domain constraint of Eq. (2) to produce new estimates of f and g, $\tilde{f}_k$ and $\tilde{g}_k$, respectively, at each iteration. Note that each AD loop produces two estimates of F (and G): (1) $\tilde{F}_k$, the Fourier transform of $\tilde{f}_k$, and (2) the estimate obtained by imposing the Fourier-domain constraint of Eq. (2). These two estimates are averaged by using the scalar β $(0 < \beta < 1)$ to form F_k, a composite estimate of F. Ayers and Dainty proposed the following estimate of F from $\tilde{F}_k$ and $\tilde{G}_k$, the Fourier transform of $\tilde{g}_k$:

if $|C(\bar{u})| <$ noise level,

$$F_k(\bar{u}) = \tilde{F}_k(\bar{u}); \tag{5a}$$

0740-3232/90/030428-06$02.00

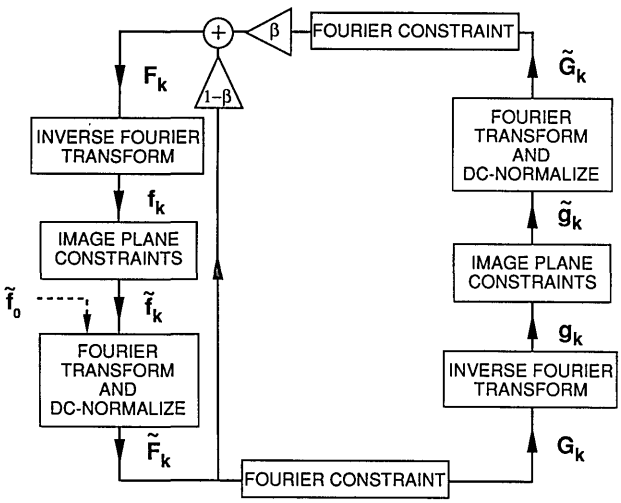

Fig. 1. AD blind deconvolution algorithm.

if $|G_k(\bar{u})| > |C(\bar{u})|$,

$$F_k(\bar{u}) = (1-\beta)\tilde{F}_k(\bar{u}) + \beta\frac{C(\bar{u})}{\tilde{G}_k(\bar{u})}; \tag{5b}$$

if $|G_k(\bar{u})| < |C(\bar{u})|$,

$$\frac{1}{F_k(\bar{u})} = \frac{1-\beta}{\tilde{F}_k(\bar{u})} + \beta\frac{\tilde{G}_k(\bar{u})}{C(\bar{u})}. \tag{5c}$$

Rather than implementing Eqs. (5), we use a Wiener-type filter based on the following imaging model:

$$c(\bar{x}) = s(\bar{x}) * f(\bar{x}) + n(\bar{x}), \tag{6}$$

or in the Fourier domain

$$C(\bar{u}) = S(\bar{u})F(\bar{u}) + N(\bar{u}), \tag{7}$$

where c is the measured image, f is the object, s is the impulse response [the Fourier transform of which is $S(\bar{u})$, the optical transfer function], and n is the noise. Assuming that f and n are independent, zero-mean, Gaussian random processes, the minimum mean-squared-error linear estimator for $f(\bar{x})$ is[5] $\hat{f}(\bar{x}) = \mathcal{F}^{-1}[\hat{F}(\bar{u})]$, where

$$\hat{F}(\bar{u}) = W(\bar{u})C(\bar{u}), \tag{8}$$

the Wiener–Helstrom filter is

$$W(\bar{u}) = \frac{S^*(\bar{u})}{|S(\bar{u})|^2 + \langle|N(\bar{u})|^2\rangle/\langle|F(\bar{u})|^2\rangle}, \tag{9}$$

and $\langle|N(\bar{u})|^2\rangle$ and $\langle|F(\bar{u})|^2\rangle$ are the ensemble-averaged energy spectra of the noise and the object, respectively. Although the images generally will not satisfy the statistical assumptions stated above, the filter is still effective and simple to implement. The Wiener–Helstrom filter of Eq. (9) is often used for image restoration.

To apply Eq. (9) to the problem of estimating F from C and $\tilde{G}$, we relate Eq. (2) to Eq. (7) [and, hence, Eq. (1) to Eq. (6)] by allowing $G(\bar{u})$ to play the role of $S(\bar{u})$. The resulting Fourier-domain constraint (with $\beta = 1$) is

$$F_k(\bar{u}) = \frac{\tilde{G}_k^*(\bar{u})}{|\tilde{G}_k(\bar{u})|^2 + \sigma^2/|\tilde{F}_k(\bar{u})|^2}C(\bar{u}), \tag{10}$$

where $\tilde{G}_k$ is the latest estimate of G, the constant σ^2 is an estimate of $\langle|N|^2\rangle$, and $|\tilde{F}_k|^2$ is used to estimate $\langle|F|^2\rangle$. A filter similar to this was used with the AD algorithm by Davey *et al.*[6] for the blind deconvolution of noisy, complex-valued images. We have approximated $\langle|N|^2\rangle$ with a constant based on the assumption that $n(\bar{x})$ is a delta-correlated, Gaussian random process. If the ensemble-averaged energy spectrum of the noise is known, it should replace σ^2 in Eq. (10).

To estimate G from C and $\tilde{F}_k$, the latest estimate of F, in Eq. (10) we replace F_k with G_k, $\tilde{G}_k$ with $\tilde{F}_k$, and, following the indexing of Fig. 1, $\tilde{F}_k$ with $\tilde{G}_{k-1}$:

$$G_k(\bar{u}) = \frac{\tilde{F}_k^*(\bar{u})}{|\tilde{F}_k(\bar{u})|^2 + \sigma^2/|\tilde{G}_{k-1}(\bar{u})|^2}C(\bar{u}). \tag{11}$$

We have also used an even simpler Wiener-type filter, formed by replacing the term $\sigma^2/|\tilde{F}_k|^2$ in the denominator of Eq. (10) with a constant, α:

$$F_k(\bar{u}) = \frac{\tilde{G}_k^*(\bar{u})}{|\tilde{G}_k(\bar{u})|^2 + \alpha}C(\bar{u}). \tag{12}$$

We will refer to this simpler filter as AD Filter 1, and the filter in Eq. (10) as AD Filter 2. We make the same substitutions that are made for Eq. (10) to obtain the following expression for $G_k(\bar{u})$ from Eq. (12):

$$G_k(\bar{u}) = \frac{\tilde{F}_k^*(\bar{u})}{|\tilde{F}_k(\bar{u})|^2 + \alpha}C(\bar{u}). \tag{13}$$

B. Phase Retrieval

As we noted in Section 1, phase retrieval can be viewed as the process of blindly deconvolving a function $f(\bar{x})$ and its twin, $f^*(-\bar{x})$. Thus for phase retrieval the noisy measurements of $r(\bar{x})$ and $|F(\bar{u})|^2$ take on the roles of $c(\bar{x})$ and $C(\bar{u})$, respectively, and $F_k(\bar{u})$ and $G_k(\bar{u})$ become estimates of $F(\bar{u})$ and $F^*(\bar{u})$, respectively. Because the two convolution factors are twins, the AD algorithm actually produces two estimates of f per iteration. Therefore we need only consider half of the AD loop (Fig. 2); i.e., instead of estimating $F^*(\bar{u})$ and $f^*(-\bar{x})$ we forego the second half of the loop and find a new estimate of $F(\bar{u})$ by conjugating $G_k(\bar{u})$, the estimate of $F^*(\bar{u})$. Replacing C with $|F|^2$, we conjugate Eq. (13) to obtain the AD Filter 1 phase-retrieval Fourier-domain constraint:

$$F_k(\bar{u}) = \tilde{G}_k^*(\bar{u}) = \frac{\tilde{F}_k(\bar{u})}{|\tilde{F}_k(\bar{u})|^2 + \alpha}|F(\bar{u})|^2. \tag{14}$$

AD Filter 2 is modified in a similar manner by conjugating Eq. (11) and substituting $|\tilde{F}_k|^2$ for $|\tilde{G}_{k-1}|^2$:

$$F_k(\bar{u}) = \frac{\tilde{F}_k(\bar{u})}{|\tilde{F}_k(\bar{u})|^2 + \sigma^2/|\tilde{F}_k(\bar{u})|^2}|F(\bar{u})|^2. \tag{15}$$

Note that for photon (shot) noise in the measurement of $C(\bar{u})$, which would have a variance proportional to the mean of $|F|^2$, the quantity $\sigma^2/|\tilde{F}(\bar{u})|^2$ is equivalent to α in Eq. (14).

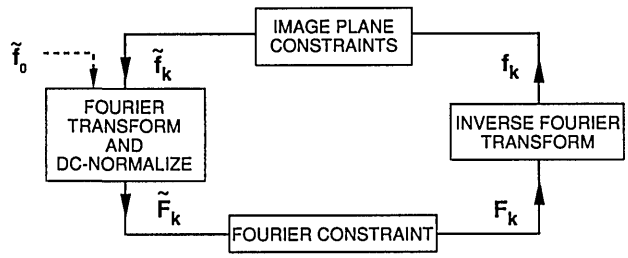

Fig. 2. AD blind deconvolution algorithm applied to phase retrieval.

C. Comparison with Error Reduction

The flow chart in Fig. 2 of the AD algorithm applied to phase retrieval is identical in form to the ER algorithm. The difference between the ER algorithm and the AD algorithm lies with the Fourier-domain constraint. In the ER algorithm the Fourier-domain constraint is imposed by substituting the known modulus, $|F(\bar{u})|$, for $|\tilde{F}_k(\bar{u})|$, the modulus of the Fourier transform of $\tilde{f}_k(\bar{x})$, the estimate of the object. If we write $\tilde{F}_k(\bar{u}) = |\tilde{F}_k(\bar{u})| \exp[i\Phi_k(\bar{u})]$, then the Fourier-domain step in the ER algorithm gives

$$F_k(\bar{u}) = |F(\bar{u})|\exp[i\Phi_k(\bar{u})] = \tilde{F}_k(\bar{u}) \frac{|F(\bar{u})|}{|\tilde{F}_k(\bar{u})|}. \tag{16}$$

If for simplicity we assume that we are using an inverse filter [which corresponds to the noise-free case and is obtained by setting $\alpha = 0$ in Eq. (14) or $\sigma = 0$ in Eq. (15)], then the AD Fourier-domain constraint can be written as

$$F_k(\bar{u}) = \tilde{F}_k(\bar{u}) \frac{|F(\bar{u})|^2}{|\tilde{F}_k(\bar{u})|^2}. \tag{17}$$

Comparison of Eqs. (16) and (17) shows that, for the noise-free case, the Fourier-domain constraint of the AD algorithm is similar to that of the ER algorithm: they both produce estimates with the same phase, and the magnitudes of both estimates are boosted (or attenuated) where $|F|/|\tilde{F}_k| > 1$ (or < 1). Because the object-domain operations are identical and the Fourier-domain constraints are so similar, we expect the AD and ER algorithms to behave similarly.

3. EXPERIMENTAL SIMULATIONS

The two versions of the AD algorithm (AD Filters 1 and 2) were compared experimentally with each other, with ER, and with a combination of HIO and ER (HIO/ER) for two cases: (1) a real-valued, nonnegative object with *a priori* known triangular support of side 128 pixels embedded in a 256 × 256 array and (2) a real-valued, nonnegative object with unknown support (approximately 40 × 60 pixels) in a 128 × 128 array. The triangular support in case (1) was chosen to allow for rapid convergence even for the slower algorithms.[7] For case (1) we also added Gaussian noise to the Fourier intensity data. The reconstructions for case (2) are more difficult because the support is unknown and because it is of a less-favorable shape.[7] For each case, the same initial guess is used to begin all the algorithms.

A useful error metric for measuring the success of the reconstruction is the normalized root-mean-squared (NRMS) error with the original object. This error metric takes advantage of the fact that, in a simulation like this, we know the original object, $f(\bar{x})$. Recalling that the estimate of $f(\bar{x})$ after the kth iteration is $\tilde{f}_k(\bar{x})$, we define the NRMS error,

$$\text{ABSERR} \equiv \left[\frac{\sum_{\bar{x}} |\alpha \tilde{f}_k(\bar{x} - \bar{x}_0) - f(\bar{x})|^2}{\sum_{\bar{x}} |f(\bar{x})|^2} \right]^{1/2}, \tag{18}$$

where x_0 maximizes the cross correlation between f and $\tilde{f}_k$ and

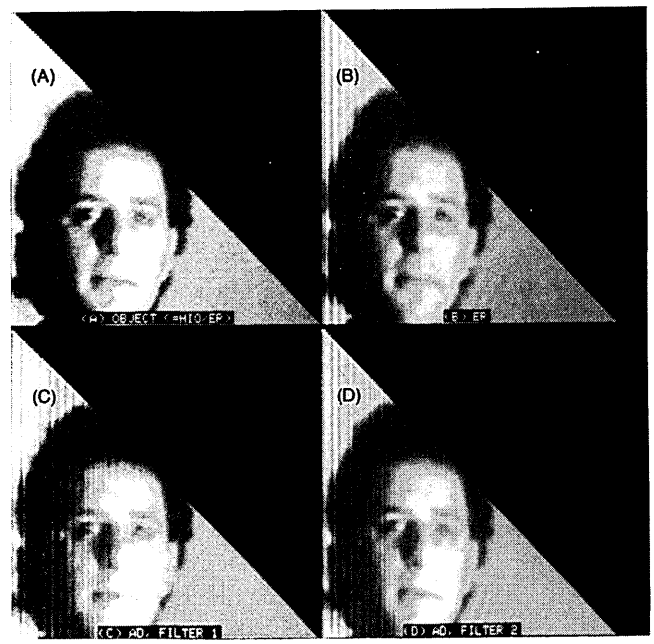

Fig. 3. Comparison of phase-retrieval using AD blind deconvolution with the HIO and ER iterative transform algorithms for a real-valued, nonnegative object with known support and no Fourier modulus error. Reconstructed images: (A) HIO/ER (indistinguishable from the original object); (B) ER; (C) AD with the Fourier constraint of Eq. (14); (D) AD with the Fourier constraint of Eq. (15).

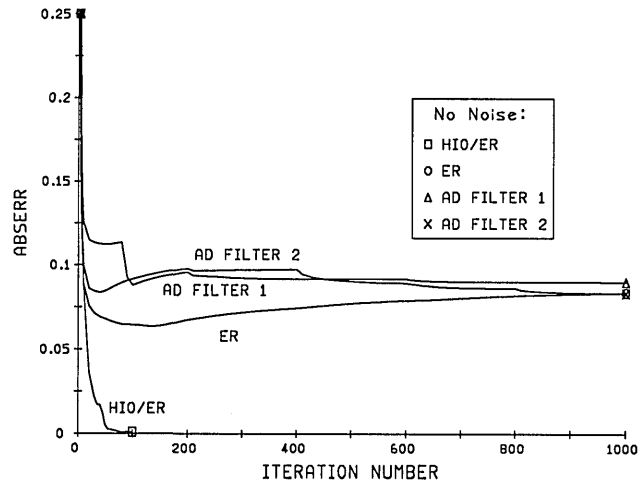

Fig. 4. ABSERR versus iteration number for the reconstructions of Fig. 3.

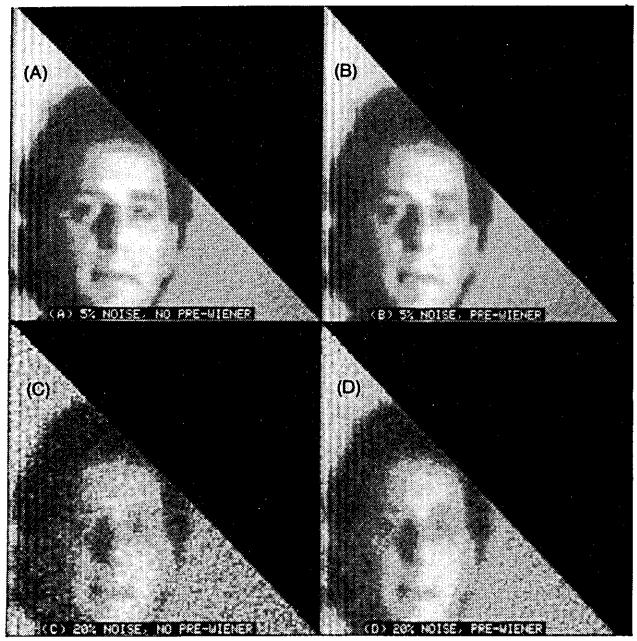

Fig. 5. Comparison of the effect of the pre-Wiener filtering of noisy Fourier intensity data on reconstructions with the ER algorithm. Reconstructed images after 1000 iterations: (A) 5% FME, no pre-Wiener filtering; (B) 5% FME, pre-Wiener filtering; (C) 20% FME, no pre-Wiener filtering; (D) 20% FME, pre-Wiener filtering.

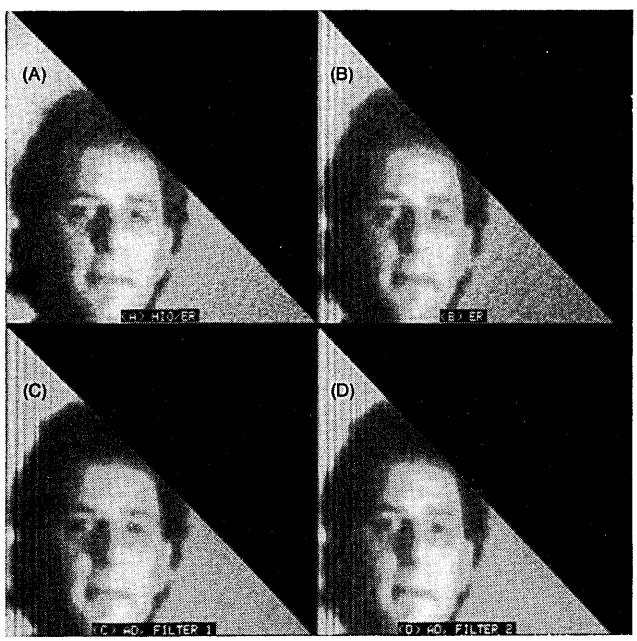

Fig. 6. Comparison of phase retrieval using AD, HIO, and ER for a real-valued, nonnegative object with known support and 5% FME. Reconstructed images: (A) HIO/ER, (B) ER, (C) AD with the Fourier constraint of Eq. (14), (D) AD with the Fourier constraint of Eq. (15).

$$\alpha = \frac{\sum_{\bar{x}} f(\bar{x}) \tilde{f}_k^*(\bar{x} - \bar{x}_0)}{\sum_{\bar{x}} |\tilde{f}_k(\bar{x})|^2} \tag{19}$$

is a scalar that can be shown to minimize ABSERR.

The reconstructions for case (1) with noise-free Fourier intensity data are shown in Fig. 3 [AD Filter 1 corresponds to Eq. (14), and AD Filter 2 to Eq. (15)]. The ER and AD images exhibit similar striping artifacts, which are frequently seen in iterative reconstruction.[4] Methods developed for eliminating the stripes[4] were not attempted here. The HIO/ER image avoids this stagnation effect and converges more quickly to a solution indistinguishable from the original object. Figure 4 is a plot of ABSERR versus iteration number for the reconstructions of Fig. 3. The AD and ER algorithms stagnated after approximately 50 iterations, while HIO/ER converged to the solution in fewer than 100 iterations. Because we used filter parameters α and σ^2 that were

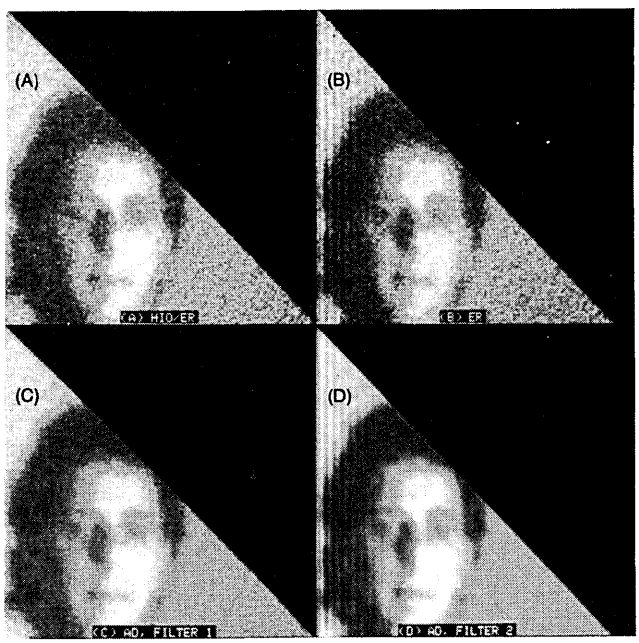

Fig. 7. Comparison of phase retrieval using AD, HIO, and ER for a real-valued, nonnegative object with known support and 20% FME. Reconstructed images: (A) HIO/ER, (B) ER, (C) AD with the Fourier constraint of Eq. (14), (D) AD with the Fourier constraint of Eq. (15).

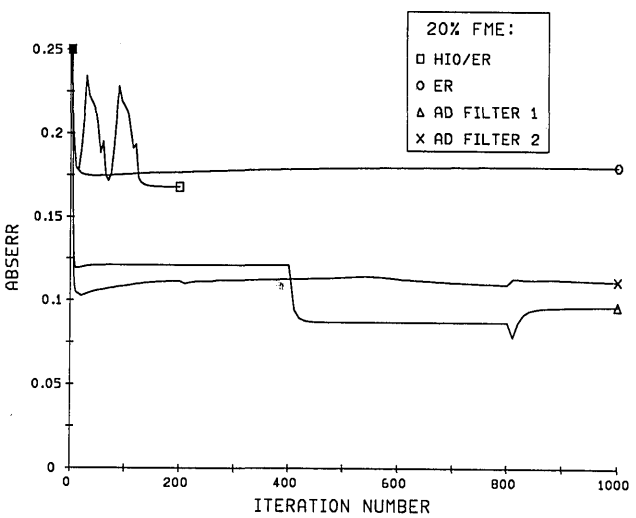

Fig. 8. ABSERR versus iteration number for the reconstructions of Fig. 7.

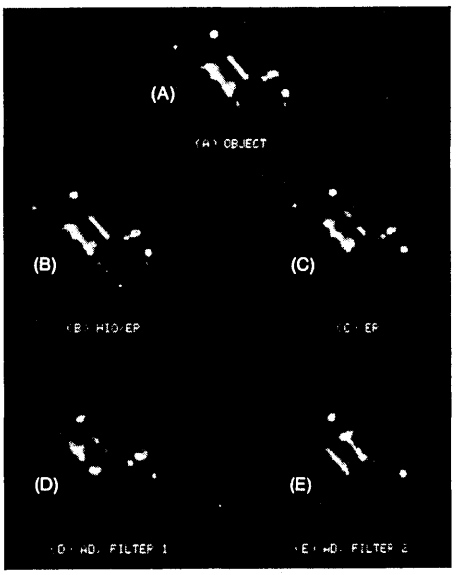

Fig. 9. Comparison of phase retrieval using AD, HIO, and ER for a real-valued, nonnegative object with unknown support and no FME. (A) Object. Reconstructed images: (B) HIO/ER, (C) ER, (D) AD with the Fourier constraint of Eq. (14), (E) AD with the Fourier constraint of Eq. (15).

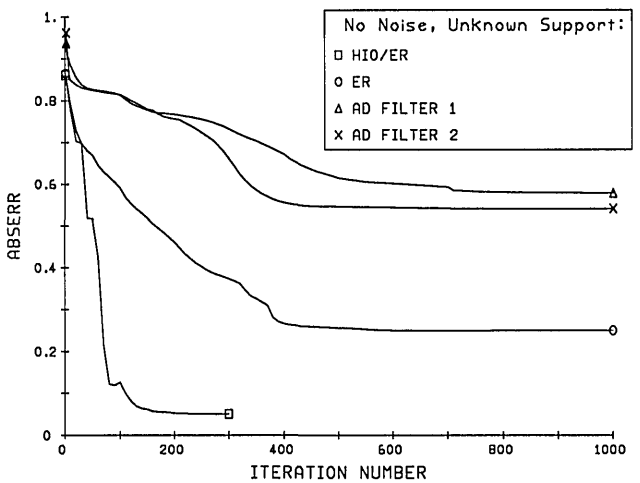

Fig. 10. ABSERR versus iteration number for the reconstructions of Fig. 9.

small (to account for computer roundoff error) for the noiseless case, there is little difference between the two AD filters, and the corresponding reconstructions are almost identical. We expect the differences between the filters to become more apparent for the case of noisy Fourier intensity data.

We now consider the same image with Gaussian noise added to the Fourier intensity. When the noisy Fourier intensity is denoted by $|F(\bar{u})|_n^2$, the Fourier-modulus error (FME) with respect to the original Fourier intensity, $|F(\bar{u})|^2$, is

$$\mathrm{FME} \equiv \left\{ \frac{\sum_{\bar{u}} [|F(\bar{u})|_n - |F(\bar{u})|]^2}{\sum_{\bar{u}} |F(\bar{u})|^2} \right\}^{1/2}. \tag{20}$$

We performed reconstructions for single realizations of $|F|_n^2$ with 5% and 20% FME. Because the AD algorithm has a Wiener-type filter built into it, a less-prejudiced comparison between algorithms is obtained if we filter the noisy Fourier intensity before use with the ER and HIO algorithms. The pre-Wiener-filtered modulus that is used in this case is

$$|\hat{F}(\bar{u})| = \left[\frac{1}{1 + \sigma^2/|F(\bar{u})|_n^4} |F(\bar{u})|_n^2 \right]^{1/2}, \tag{21}$$

where σ^2 is the variance of the noise added to the Fourier intensity. Figure 5 demonstrates the effect of Eq. (21) on ER reconstructions for the two noisy cases. The smoothing of the pre-Wiener filter has a negligible effect for the 5% FME data but is more significant for the 20% FME data.

The reconstructions from all four algorithms for the case of 5% FME are shown in Fig. 6. Since the pre-Wiener filtering of Eq. (21) was insignificant at the 5% FME noise level, it was not used in these HIO and ER reconstructions. The 5% level of noise has little effect on visual image quality, and the performance of the algorithms relative to one another is similar to that for the noiseless case. Reconstructions with 20% FME are shown in Fig. 7. This level of noise significantly degrades the visual image quality, and the pre-Wiener filtering was implemented for the HIO and ER reconstructions. The AD Filter 1 image of Fig. 7(C) has no striping artifacts and is comparable in quality with the HIO/ER reconstruction of Fig. 7(A), whereas AD Filter 2 stagnates with stripes after starting with the same initial guess. The low-pass nature of the Wiener-type filter has a smoothing effect that is evident in the AD reconstructions. The amount of smoothing depends on the filter parameters α and σ^2: the larger these parameter are, the larger the attenuation of high frequencies and the smoother the reconstruction. In this case the two AD reconstructions achieve a smaller ABSERR than either ER or HIO/ER (Fig. 8) but at the expense of image sharpness. The reconstructions stagnate almost immediately, but a change in α after 400 iterations moves the AD Filter 1 image out of stripe stagnation. The ability to vary the built-in Wiener-type filter parameters may be an advantage of the AD algorithm. The AD algorithm also may be making better use of the Wiener filter, and a few iterations of AD Filter 1 on the HIO/ER image of Fig. 7(A) yields an image that is similar to that in Fig. 7(C).

Figure 9 shows the reconstructions from all four algorithms for case (2), a real-valued, nonnegative image with unknown support in a 128 × 128 array. The support was estimated from the support of the autocorrelation, $r(\bar{x})$, using a triple-intersection algorithm.[8] Figure 10 is a plot of ABSERR versus iteration number for the reconstructions of Fig. 9. The HIO/ER algorithm converged close to the solution in fewer than 200 iterations, whereas AD and ER both converged more slowly and stagnated after approximately 400 iterations. The error of the ER reconstruction is significantly lower than that of the AD algorithms. For this more-difficult case, we find again that the AD and ER algorithms perform comparably (ER somewhat better than AD), and HIO/ER is still more effective than either.

4. CONCLUSION

We have shown that the Ayers–Dainty (AD) blind deconvolution algorithm applied to phase retrieval is similar to the error-reduction (ER) iterative Fourier-transform algorithm, both in form and in performance. A nice feature of the AD

algorithm is a built-in Wiener-type filter, which seems to perform slightly better than the pre-Wiener filter used with hybrid input–output (HIO) and ER for the noisier case. The two different Wiener-type filters considered here performed comparably, and the significant difference between them is that Filter 1 [Eq. (14)] is simpler to implement than Filter 2 [Eq. (15)]. For the more difficult case of reconstructing an object with unknown support, the AD algorithm was not quite so effective as ER and did not converge close to a solution as did the combination of HIO and ER (HIO/ER). HIO/ER is still the most effective reconstruction algorithm at low noise levels, and at higher levels of noise the AD algorithm can be used in conjunction with HIO to improve the quality of the reconstruction.

ACKNOWLEDGMENTS

This research was supported by the U.S. Office of Naval Research under contract N00014-86-C-0587.

Portions of this paper were presented at the Optical Society of America Topical Meeting on Signal Recovery and Synthesis III, North Falmouth, Massachusetts, June 14–16, 1989.[9]

REFERENCES

1. G. R. Ayers and J. C. Dainty, "An iterative blind deconvolution method and its applications," Opt. Lett. **13,** 547–549 (1988).
2. J. R. Fienup, "Reconstruction of an object from the modulus of its Fourier transform," Opt. Lett. **3,** 27–29 (1978).
3. J. R. Fienup, "Phase retrieval algorithms: a comparison," Appl. Opt. **21,** 2758–2769 (1982).
4. J. R. Fienup and C. C. Wackerman, "Phase-retrieval stagnation problems and solutions," J. Opt. Soc. Am. A **3,** 1897–1907 (1986).
5. C. W. Helstrom, "Image restoration by the method of least squares," J. Opt. Soc. Am. **57,** 297–303 (1967).
6. B. L. K. Davey, R. G. Lane, and R. H. T. Bates, "Blind deconvolution of noisy complex-valued image," Opt. Commun. **69,** 353–356 (1989). In Eq. (15) of that paper, by our logic, the term $\alpha/|F_{i-1}(u)|^2$ in the denominator should be $\alpha/|H_{i-1}(u)|^2$.
7. J. R. Fienup, "Reconstruction of a complex-valued object from the modulus of its Fourier transform using a support constraint," J. Opt. Soc. Am. A **4,** 118–123 (1987).
8. T. R. Crimmins, J. R. Fienup, and B. J. Thelen, "Improved bounds on object support from autocorrelation support and application to phase retrieval," J. Opt. Soc. Am. A **7,** 1–13 (1990).
9. J. H. Seldin and J. R. Fienup, "Phase retrieval using Ayers/Dainty deconvolution," in *Digest of Topical Meeting on Signal Recovery and Synthesis III* (Optical Society of America, Washington, D.C., 1989), pp. 124–127.